Effects of planet curvature and crust on the shock pressure field around impact basins

Karin L. Louzada[1] and Sarah T. Stewart[1]

Received 21 February 2009; revised 1 July 2009; accepted 6 July 2009; published 7 August 2009.

[1] We investigate the effects of planetary curvature and the crust-mantle boundary on the shock pressure field around impact basins on Mars using acoustic ray path calculations and hydrocode simulations. Planet curvature and, to a lesser extent, increasing sound speed with depth shallow the zone of wave interference, where shock pressures decay rapidly to the surface. The depth to the interference zone boundary diverges from the flat surface solution for projectile-to-Mars radius ratios greater than ~1% (transient craters greater than ~300 km); the difference increases with distance from the impact point and projectile size. In hydrocode simulations (but not the simple ray path model), the presence of the crust-mantle boundary produces nearly vertical pressure contours in the crust. Around Hellas basin, demagnetization occurs at shock pressures between 1.1 (±0.2) and 3.4 (±0.7) GPa, where the range is due to the uncertainty in the transient crater diameter. **Citation:** Louzada, K. L., and S. T. Stewart (2009), Effects of planet curvature and crust on the shock pressure field around impact basins, *Geophys. Res. Lett.*, *36*, L15203, doi:10.1029/2009GL037869.

1. Introduction

[2] Recent interest in the shock pressure field around impact basins has been fueled by observations of unmagnetized crust around the younger basins on Mars [e.g., Hellas basin, *Acuña et al.*, 1999] coupled with experimental evidence of pressure demagnetization of magnetic minerals at a few GPa [e.g., *Hargraves and Perkins*, 1969; *Nagata*, 1974; *Cisowski and Fuller*, 1978; *Rochette et al.*, 2003; *Kletetschka et al.*, 2004; *Gattacceca et al.*, 2007; *Louzada et al.*, 2007]. It is hoped that understanding shock demagnetization will provide constraints on the mineralogy of the crust [*Cisowski and Fuller*, 1978; *Kletetschka et al.*, 2004; *Bezaeva et al.*, 2007].

[3] Near the surface around impact craters, compressive waves and rarefaction waves reflected from the planet's surface interact, leading to a zone of reduced shock pressure [*Melosh*, 1984]. The shock pressure distribution in the crust is sensitive to the geometry of this interference zone. Previous estimates of the shock pressure distribution in the crust surrounding Martian impact basins have not included an interference zone [*Hood et al.*, 2003] or used an adaptation of the stress wave propagation and reflection model for flat homogeneous surfaces by *Melosh* [1984] [e.g., *Kletetschka et al.*, 2004; *Mohit and Arkani-Hamed*, 2004].

[4] In this work, we investigate the effects of planet curvature and the crust-mantle boundary on the geometry of the interference zone and the shock pressure distribution in the crust around large impact events. We perform numerical wave propagation calculations and solve for shock pressures in the interference zone. We compare ray path results for a Hellas-size event to two- and three-dimensional simulations using the hydrocode CTH [*McGlaun et al.*, 1990]. Finally, we discuss the implications for shock demagnetization on Mars.

2. Method: Near-Surface Pressure Field

2.1. Interference Zone Boundary for a Flat Surface

[5] The stress wave propagation and reflection model of *Melosh* [1984] likens the impact to an explosion centered at burial depth, d. At any point in the subsurface, shock waves emitted from this point are followed by reflected waves from the planet's surface with an arrival time delay, Δt. The pressure history of the material can be approximated as the sum of the two waves (Figure 1). In the interference zone, the arrival time difference between the two waves is less than the shock rise time ($\Delta t < \tau$), and the peak shock pressure is reduced. The interference zone boundary is defined where $\Delta t = \tau$.

[6] *Melosh* [1984] calculated the depth of the interference zone boundary (D_{IZB}) as a function of distance along the surface, s:

$$D_{\mathrm{IZB}}(s) = c_{\mathrm{L}}\tau\left[\left(4\left(d^2+s^2\right)-c_{\mathrm{L}}^2\tau^2\right)\Big/\left(4d^2-c_{\mathrm{L}}^2\tau^2\right)\right]^{1/2}. \quad (1)$$

τ is approximated by $r_{\mathrm{pr}}/v_{\mathrm{i}}$; r_{pr} is the projectile radius, v_{i} is the impact velocity and $d = 0.7{\cdot}r_{\mathrm{pr}}$ [*Pierazzo et al.*, 1997]. The waves are assumed to travel at a constant longitudinal sound speed, c_{L}.

[7] Previous pressure field estimates around impact basins on Mars using equation (1) differed in (1) the value of d, (2) the impact conditions (projectile diameter and velocity), and (3) the method for calculating the reduced pressure in the interference zone, either a linear decay to the surface from the maximum pressure at depth [*Kletetschka et al.*, 2004] or summing of two triangular-shaped waves (a function of Δt and τ [*Mohit and Arkani-Hamed*, 2004]). These studies did not include two potentially important factors. First, due to curvature of the planet's surface, the difference in path length (and arrival time) between the direct and reflected waves is larger in a spherical planet than in a flat planet (Figure S1, auxiliary material).[2] Second, the interference zone may be affected by variable wave speeds and the presence of the crust-mantle boundary.

[1]Department of Earth and Planetary Sciences, Harvard University, Cambridge, Massachusetts, USA.

0094-8276/09/2009GL037869$05.00

[2]Auxiliary materials are available in the HTML. doi:10.1029/2009GL037869.

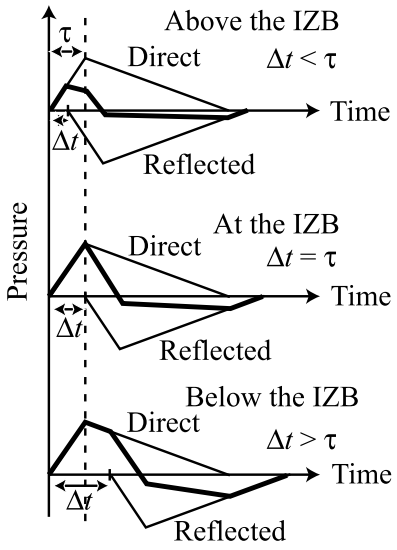

Figure 1. Schematic of interaction between triangular-shaped direct and reflected waves above, at, and below the interference zone boundary (IZB) [after *Melosh*, 1984]. The pressure history of the material is the sum of the two waves (thick solid line).

2.2. Ray Path Model for a Spherical Planet

[8] Here, we incorporate flat and spherical planet geometries in ray path calculations to solve for the interference zone boundary. Mars is modeled with three internal structures (Figure S2): (I) homogeneous (crust only), (II) heterogeneous with a 50-km thick crust, 2000-km thick mantle, and 1376-km radius core, and (III) heterogeneous without a crust (the mantle extends to the surface). Waves are propagated radially away from the burial point and refracted or reflected according to the local longitudinal sound speed. The propagation time step is constrained by the cell size in a two-dimensional grid (rectangular or polar). In each grid cell, the arrival times and ray path lengths of the compressive and reflected waves are collected, and the depth to the interference zone boundary is determined. Grid resolution, angle spacing and time step sensitivity tests are shown in Figure S3.

2.3. Shock Pressure Decay

[9] In the ray path calculation, the amplitude of the waves is assumed to decay as a function of the total distance traveled, l. The maximum shock pressure occurs near the impact point in the isobaric core (P_{ibc}, $\sim$ 130 GPa for basaltic materials and typical impact velocities of 9 km/s for Mars [*Ivanov*, 2001]). Outside of the isobaric core, the shock pressure amplitude decays exponentially as a (segmented) power-law with distance [*Ahrens and O'Keefe*, 1987; *Pierazzo et al.*, 1997]. Figure 2 shows the results of shock pressure decay with distance from CTH simulations using the impact conditions described in section 3.1. Since we are interested in the few GPa pressure regime and *Pierazzo et al.*'s [1997] scaling laws do not extend past $5 \cdot r_{pr}$, we utilize the pressure decay results from the CTH simulations in the ray path calculations.

[10] In each grid cell, the pressures of the direct ($P > 0$) and reflected ($P < 0$) rays are determined from their path lengths and the pressure function. The effective pressure, P_{eff}, in cells located in the interference zone is a function of the arrival time difference of the waves [after *Melosh*, 1984]:

$$P_{eff} = P(l_D) + P(l_R)(1 - \Delta t/\tau), \quad (2)$$

where l_D and l_R are the total distances that the direct and reflected waves have traveled (scaled by projectile size), respectively.

3. Results

3.1. A Hellas Forming Impact

[11] Hellas is an example of a basin clearly devoid of crustal magnetization [*Acuña et al.*, 1999]. In order to derive the shock pressure field around Hellas, we need to estimate the impact conditions and therefore its transient crater. Hellas basin is elliptical with inner (floor) and outer (rim-to-rim) topographic boundaries of 1400–2000 km and 1900–2300 km, respectively. Previous workers [*Hood et al.*, 2003; *Kletetschka et al.*, 2004; *Mohit and Arkani-Hamed*, 2004] have assumed that the transient basin diameter is comparable to the inner topographic boundary ($\sim$1300–1500 km), which must be an upper limit. We initially make the same assumption here.

[12] Using Π-scaling for flat surfaces [e.g. *Melosh*, 1989, section 7.7; *Melosh and Beyer*, 1998], a 230-km radius asteroid (3000 kg/m^3) at a typical (vertical) impact velocity of 9 km/s onto Mars (3000 kg/m^3) produces a 1250-km diameter transient crater in competent rock. Hydrodynamic CTH calculations (auxiliary material) using the same impact parameters produce transient crater diameters of 1300–1400 km.

3.2. IZB for a Flat Versus Spherical Homogeneous Planet

[13] First we consider a homogenous planet (case I) to assess the effect of planet curvature. Using the ray path model, we compare the depth to the interference zone boundary, D_{IZB}, for a flat and spherical Mars. The blue dots

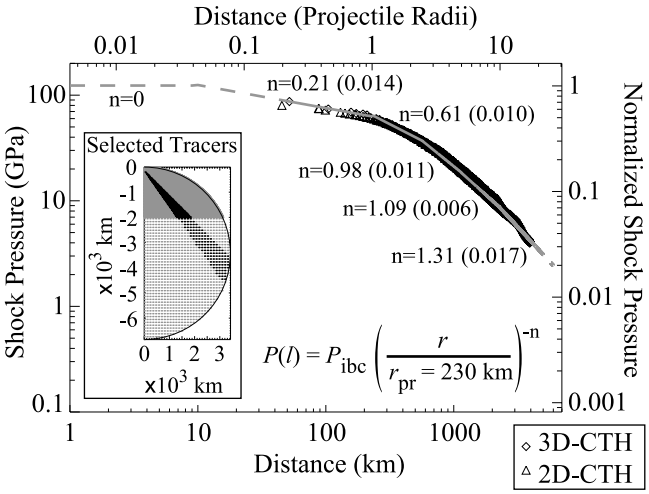

Figure 2. Shock pressure versus radial distance from a burial depth of $0.7 \cdot r_{pr}$ recorded by tracers below the interference zone in the crust and upper mantle (inset), for a 230-km radius projectile at 9 km/s. The 2D (triangles) and 3D (diamonds) results are nearly identical. Power-law exponents are indicated with standard deviations in parentheses.

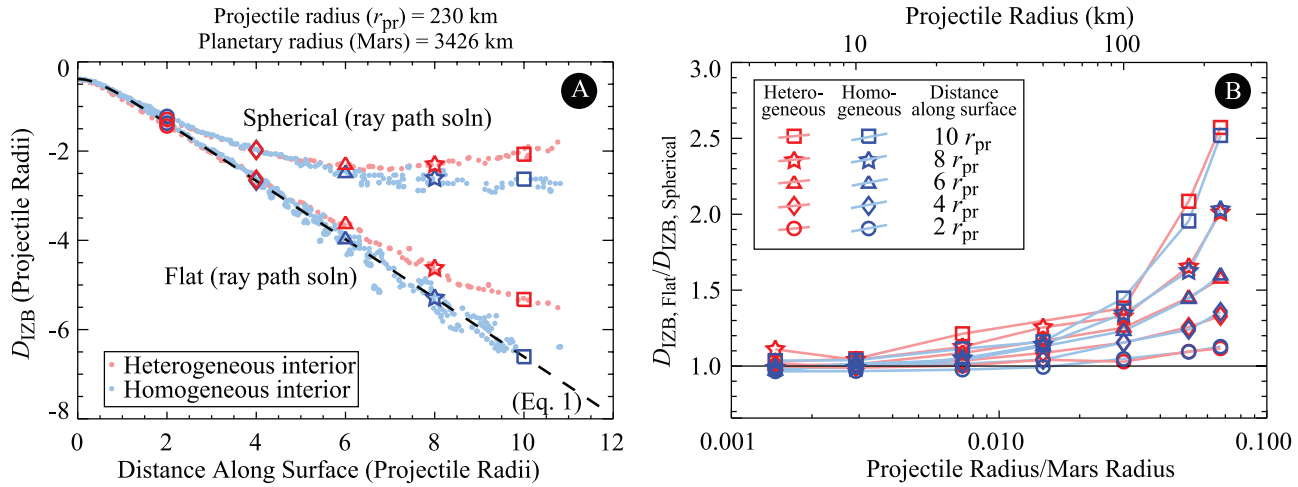

Figure 3. (a) Depth to the interference zone boundary (D_{IZB}) for a 230-km radius projectile at 9 km/s into a flat and spherical, homogeneous (case I - blue) and heterogeneous (case II - red) Mars. The correlation between the homogeneous flat planet case and equation (1) (dashed line) is $R^2 = 0.985$. (b) Ratio between $D_{IZB, Flat}$ and $D_{IZB, Sph}$ for different projectile-to-planet radius ratios (Table S3). We assume $\tau = r_{pr}/v_i$ (constant), $v_i = 9$ km/s, and $d = 0.7 \cdot r_{pr}$.

in Figure 3a show D_{IZB} for an impact on a homogeneous Mars by a 230-km radius projectile at 9 km/s (a Hellas-type event). (Note that D_{IZB} is independent of the pressure decay profile.) The results indicate that the IZB is shallower in a spherical planet and that the depth to the boundary decreases with increasing distance and impactor size (Figure 3b). For example, the IZB is reduced by approximately 40% for the Hellas-type event (a 230-km radius projectile) at a distance of ~1000 km (4 r_{pr}, right-most diamonds in Figure 3b), the radius of the demagnetized zone (see section 4.2).

3.3. IZB for a Flat Versus Spherical Heterogeneous Planet

[14] Calculations using a full Mars interior model (heterogeneous case II, red dots in Figure 3a) produce IZBs that are slightly shallower than those for a homogeneous Mars, for both spherical and flat planet geometries. The depth to the IZB is more sensitive to the planet curvature than the increasing longitudinal sound speed with depth. In fact, the change in depth of the IZB due to planet geometry is nearly independent of the internal structure of the planet for all projectile radii and distances (compare the red and blue symbols in Figure 3b).

3.4. Pressure Field Around Hellas Basin and the Effect of the Crust-Mantle Boundary

[15] In Figure 4, we present shock pressure contours using both the ray path model (solid lines) and the CTH calculations (dashed lines), and the Hellas impact conditions described above, for the upper 100 km of a (A) flat and (B) spherical Mars. Magnetization in the lower crust of Mars has likely been reduced due to viscous relaxation in the absence of an ambient field [*Shahnas and Arkani-Hamed*, 2007]. Also, the upper crust has been demagnetized by a combination of primary impacts [*Shahnas and Arkani-Hamed*, 2007] and secondaries from impact basins greater than ~500 km diameter [*Artemieva et al.*, 2005]. It is assumed that the magnetic crust is located between 10 and 50 km depth [*Dunlop and Arkani-Hamed*, 2005] (Figure 4). In both the ray path and CTH results, the pressure contours in the spherical planet are indeed closer to the surface than in the flat planet. However, for both the flat and spherical planet, the CTH pressure contours are steeper in the crust and deeper in the mantle compared to the ray path model. In contrast, ray path and CTH simulations for flat heterogeneous planets without a crust (case III) are of similar shape (Figure S4); thus the ray path model does not adequately capture crust-mantle boundary effects.

[16] The differences between pressure contours from ray path calculations and CTH simulations are likely due to the fact that the burial depth and shock wave rise times are not truly constant. For example, the burial depth increases with decreasing shock pressure (Figure S5). Additionally, the assumption of interference of only two waves and/or the wave shape may be too simple.

4. Discussion

4.1. Implications for Impact Basin Formation

[17] The depth to the interference zone boundary begins to diverge from the flat surface solution (by more than ~10%) for projectile radii of 25 to 50 km, corresponding to a projectile-to-planet radius ratio of ~1% (Figure 3b). Using Π-scaling developed for (smaller) complex craters, vertical impacts at 9 km/s of such impactors will produce transient craters with diameters of 221 to 380 km on Mars and final crater diameters of 700 to 1300 km [*Melosh and Beyer*, 1998]. On Mars, approximately 20 craters are of this size or larger [*Frey*, 2008].

[18] The relationship between such large impact basins and the impact conditions that formed them is highly uncertain [*Melosh*, 1989, chap. 7]. Impact basins are morphologically very different from simple and complex craters, and extensive modification during collapse makes estimation of the transient crater diameter difficult. In addition, here we only consider vertical impacts; average (45°) oblique impacts

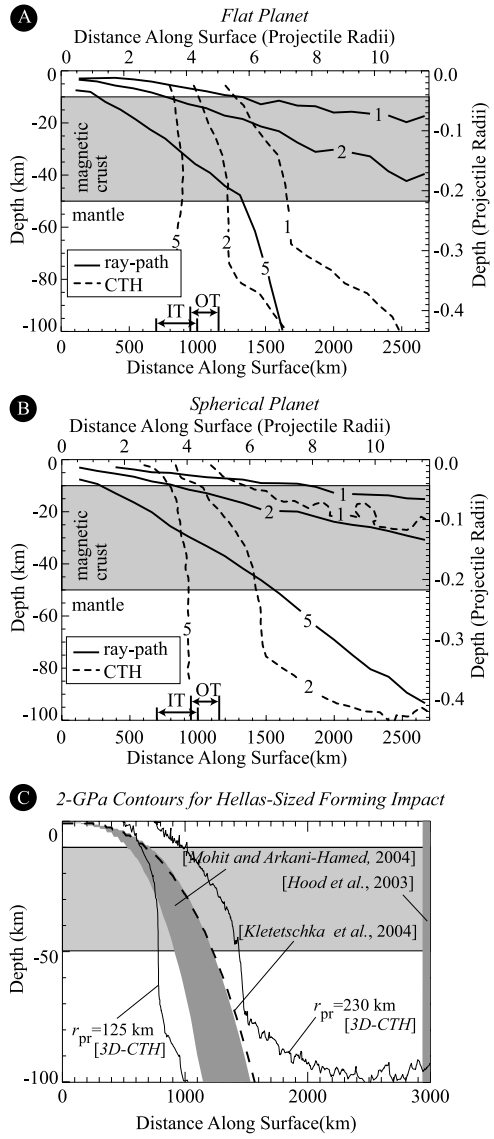

Figure 4. Shock pressure contours (5, 2, and 1 GPa) for a Hellas-size event using the ray path model (solid lines) and CTH hydrocode (dashed lines) for (a) flat and (b) spherical Mars geometries. IT and OT denote the inner and outer topographic boundaries of Hellas, respectively. (c) The 2-GPa shock pressure contours for a Hellas forming impact. See text for details. Vertical exaggeration = ~19×.

will displace the region of intense shock to shallower depths and in the downrange direction, but have little effect on the far-field lower shock pressures [*Pierazzo and Melosh*, 2000].

[19] The assumption that complex crater scaling continues into the basin regime is as valid as (and perhaps better than) the assumption of using the inner scarp to estimate the transient basin. The transient basin of Hellas was likely much smaller than its present-day flat floor. Using the geometric reconstruction for complex craters [*Melosh*, 1989, equation 8.3.1] and a basin depth of ~10 km, we estimate a lower limit for the transient basin size of Hellas at about 800 km. This value is considerably smaller than the previously assumed upper limit of 1300–1500 km. In this end-member case, using the same impact conditions, the impactor radius is only 125 km.

4.2. Implications for the Martian Magnetic Crust

[20] *Hood et al.* [2003] estimate that extensive demagnetization (~90%) occurred out to 3–4 basin radii (~2 GPa) and that significant demagnetization (~50%) occurred at 1 GPa or less (r_{pr} = 343–232 km, v_i = 7.5–15 km/s). By taking into account an interference zone, *Kletetschka et al.* [2004] estimate 60–70% impact demagnetization occurred at 1–2 basin radii (>1 GPa) (r_{pr} = 260 km, v_i = 15 km/s). Both studies assume impact angles of 45°, but symmetric pressure decay with distance. *Mohit and Arkani-Hamed* [2004] also considered an interference zone and estimated that partial demagnetization extends out to 1.2–1.4 basin radii (<0.5–1 GPa) and complete demagnetization occurred within ~0.8 basin radii (2–5 GPa) (r_{pr} = 210–230 km, v_i = 10–12 km/s). An upper limit on the radius of complete demagnetization was found by *Lillis et al.* [2009] to be 1.18 basin radii, based on modeling of crustal magnetic intensity.

[21] The 2-GPa pressure contour results from 3D-CTH simulations, using both the 230 and 125-km radius projectiles at 9 km/s, and from the previous studies are shown in Figure 4c. The results from this work bracket those of *Mohit and Arkani-Hamed* [2004] and *Kletetschka et al.* [2004]. If demagnetization extends out to 1.4 basin radii, then at a radius of ~1000 km around Hellas the average shock pressure in the magnetic portion of the crust is between 1.1 (±0.2) and 3.4 (±0.7) GPa from CTH simulations, depending on the impactor size (Table S4). All candidate magnetic minerals (magnetite, hematite and pyrrhotite [*Dunlop and Arkani-Hamed*, 2005]) demagnetize in this pressure range (summarized by *Louzada* [2009]). Considering the uncertainties in the transient basin diameter, at present, it is not possible to constrain impact demagnetization pressures and the magnetic mineralogy on Mars more precisely.

5. Conclusions

[22] The onset of shallowing of the interference zone due to curvature begins at projectile-to-planet radius ratios of ~1%. Increasing sound speeds with depth results in additional shallowing of the interference zone with respect to homogeneous planets, but to a lesser extent. Shallowing of the interference zone leads to larger average shock pressures in the crust. These trends are observed in both ray path calculations and hydrocode simulations of impact basin formation. However, modification of the shape of shock pressure contours by the crust-mantle boundary is not captured in the ray path model. Based on the range of possible transient basin diameters and impact conditions, shock demagnetization around Martian impact basins occurred between 1.1 (±0.2) and 3.4 (±0.7) GPa.

[23] **Acknowledgments.** Thanks to C. Dalton, D. Valencia, the Barringer Family Fund, the Amelia Earhart Fellowship (Zonta Int.), and two anonymous reviewers.

References

Acuña, M. H., et al. (1999), Global distribution of crustal magnetization discovered by the Mars Global Surveyor MAG/ER experiment, *Science*, *284*, 790–793, doi:10.1126/science.284.5415.790.

Ahrens, T. J., and J. D. O'Keefe (1987), Impact on the Earth, ocean and atmosphere, *Int.J. Impact Eng.*, *5*, 13–32, doi:10.1016/0734-743X(87)90028-5.

Artemieva, N, L. Hood, and B. A. Ivanov (2005), Impact demagnetization of the Martian crust: Primaries versus secondaries, *Geophys. Res. Lett.*, *32*, L22204, doi:10.1029/2005GL024385.

Bezaeva, N. S., P. Rochette, J. Gattacceca, R. A. Sadykov, and V. I. Trukhin (2007), Pressure demagnetization of the Martian crust: Ground truth from SNC meteorites, *Geophys. Res. Lett.*, *34*, L23202, doi:10.1029/2007GL031501.

Cisowski, S. M., and M. Fuller (1978), The effect of shock on the magnetism of terrestrial rocks, *J. Geophys. Res.*, *83*, 3441–3458, doi:10.1029/JB083iB07p03441.

Dunlop, D. J., and J. Arkani-Hamed (2005), Magnetic minerals in the Martian crust, *J. Geophys. Res.*, *110*, E12S04, doi:10.1029/2005JE002404.

Frey, H. (2008), Ages of very large impact basins on Mars: Implications for the late heavy bombardment in the inner solar system, *Geophys. Res. Lett.*, *35*, L13203, doi:10.1029/2008GL033515.

Gattacceca, J., A. Lamali, P. Rochette, M. Boustie, and L. Berthe (2007), The effects of explosive-driven shocks on the natural remanent magnetization and the magnetic properties of rocks, *Phys. Earth Planet. Inter.*, *162*, 85–98, doi:10.1016/j.pepi.2007.03.006.

Hargraves, R. B., and W. E. Perkins (1969), Investigations of the effect of shock on natural remanent magnetization, *J. Geophys. Res.*, *74*, 2576–2589, doi:10.1029/JB074i010p02576.

Hood, L. L., N. C. Richmond, E. Pierazzo, and P. Rochette (2003), Distribution of crustal magnetic fields on Mars: Shock effects of basin-forming impacts, *Geophys. Res. Lett.*, *30*(6), 1281, doi:10.1029/2002GL016657.

Ivanov, B. A. (2001), Mars/Moon cratering rate ratio estimates, *Space Sci. Rev.*, *96*, 87–104, doi:10.1023/A:1011941121102.

Kletetschka, G., J. E. P. Connerney, N. F. Ness, and M. H. Acuña (2004), Pressure effects on Martian crustal magnetization near large impact basins, *Meteorit. Planet. Sci.*, *39*, 1839–1848.

Lillis, R. J., J. S. Halekas, K. L. Louzada, S. T. Stewart, and M. Manga (2009), Impact demagnetization at Mars: Using multiple altitude magnetic field data to constrain properties of crustal magnetization, *Lunar Planet. Sci.* [CD-ROM], *XL*, Abstract 1444.

Louzada, K. L. (2009), The effects of impact cratering on planetary crustal magnetism, Ph.D. thesis, 240 pp., Harvard Univ., Cambridge, Massachusetts.

Louzada, K. L., S. T. Stewart, and B. P. Weiss (2007), Effect of shock on the magnetic properties of pyrrhotite, the Martian crust, and meteorites, *Geophys. Res. Lett.*, *34*, L05204, doi:10.1029/2006GL027685.

McGlaun, J. M., S. L. Thompson, and M. G. Elrick (1990), CTH: A 3-dimensional shock-wave physics code, *Int. J. Impact Eng.*, *10*, 351–360, doi:10.1016/0734-743X(90)90071-3.

Melosh, H. J. (1984), Impact ejection, spallation, and the origin of meteorites, *Icarus*, *59*, 234–260, doi:10.1016/0019-1035(84)90026-5.

Melosh, H. J. (1989), *Impact Cratering: A Geologic Process*, 245 pp., Oxford Univ. Press, New York.

Melosh, H. J., and R. A. Beyer (1998), Crater, http://www.lpl.arizona.edu/tekton/crater.html, Lunar and Planet. Lab., Univ. of Ariz., Tucson.

Mohit, P. S., and J. Arkani-Hamed (2004), Impact demagnetization of the Martian crust, *Icarus*, *168*, 305–317, doi:10.1016/j.icarus.2003.12.005.

Nagata, T. (1974), Integrated effect of repeated mechanical shocks on shock remanent magnetization and shock demagnetization, *J. Geophys.*, *40*, 467–487.

Pierazzo, E., and H. J. Melosh (2000), Melt production in oblique impacts, *Icarus*, *145*, 252–261, doi:10.1006/icar.1999.6332.

Pierazzo, E., A. M. Vickery, and H. J. Melosh (1997), A reevaluation of impact melt production, *Icarus*, *127*, 408–423, doi:10.1006/icar.1997.5713.

Rochette, P., G. Fillion, R. Ballou, F. Brunet, B. Ouladdiaf, and L. Hood (2003), High pressure magnetic transition in pyrrhotite and impact demagnetization on Mars, *Geophys. Res. Lett.*, *30*(13), 1683, doi:10.1029/2003GL017359.

Shahnas, H., and J. Arkani-Hamed (2007), Viscous and impact demagnetization of Martian crust, *J. Geophys. Res.*, *112*, E02009, doi:10.1029/2005JE002424.

K. L. Louzada and S. T. Stewart, Department of Earth and Planetary Sciences, Harvard University, Cambridge, MA 02138, USA. (louzada@post.harvard.edu)